ANNUAL REVIEWS

Annual Review of Materials Research

Fast and Selective Ionic Transport: From Ion-Conducting Channels to Ion Exchange Membranes for Flow Batteries

Klaus-Dieter Kreuer and Andreas Münchinger

Max Planck Institute for Solid State Research, 70569 Stuttgart, Germany;
email: kreuer@fkf.mpg.de

Annu. Rev. Mater. Res. 2021. 51:21–46

The *Annual Review of Materials Research* is online at matsci.annualreviews.org

https://doi.org/10.1146/annurev-matsci-080619-010139

Keywords

ionophore, ion-conducting channel, ion exchange membrane, selectivity, ion transport, vanadium-redox-flow battery

Abstract

This review discusses selective and fast transport of ionic species (ions and their associates) through systems as diverse as ion-conducting transmembrane proteins and ion exchange membranes (IEMs) in aqueous environments, with special emphasis on the role of electrostatics, specific chemical interactions, and morphology (steric effects). Contrary to the current doctrine, we suggest that properly balanced ion-coordinating interactions are more important than steric effects for selective ion transport in biological systems. Steric effects are more relevant to the selectivity of ionic transport through IEMs. As a general rule, decreased hydration leads to higher selectivity but also to lower transport rate. Near-perfect selectivity is achieved by ion-conducting channels in which unhydrated ions transfer through extremely short hydrophobic passages separating aqueous environments. In IEMs, ionic species practically keep their hydration shell and their transport is sterically constrained by the width of aqueous pathways. We discuss the trade-off between selectivity and transport rates and make suggestions for choosing, optimizing, or developing membranes for technological applications such as vanadium-redox-flow batteries.

1. INTRODUCTION

Fast and selective transport of a particular type of ion across membranes separating aqueous media of different composition is key to essential biological and technical processes such as transmission of electrochemical signals and electrochemical energy conversion. Fast ionic transport is a characteristic property of aqueous electrolytes to which the dynamics of all species is highly coupled. Hence, the limiting equivalent conductivities of ions in aqueous environments fall into a narrow range closely related to the diffusion coefficient and fluidity of the solvent (water) through the ratio of their hydrodynamic radii. By contrast, ionic transport in the solid state requires decoupling of the ion's long-range dynamics from the dynamics of the rest of the immobile structure. This is the case in solid-state ionic conductors (solid electrolytes), which provide pathways for the diffusion of one particular type of ion. The ionic conductivity of such materials is high compared with that of most solids, but it usually remains well below the high conductivity of aqueous (liquid) electrolytes. Generally speaking, the combination of fast and selective ion transport is a rare phenomenon.

Many solid electrolytes exchange their mobile ions with different types of ions present in contacting phases (e.g., aqueous solutions). In the best case, this is a *douce* ion exchange (as observed for β″ alumina) accompanied by some lattice adaptation, leaving the structure essentially intact (1). Starting from the potassium form of β″ alumina, which is a good K^+ conductor, the material can be reversibly ion exchanged into its sodium form or any other mixed K^+/Na^+ form. For these mixed ionic forms, the conductivity is significantly lower than expected from extrapolation between the conductivities of the single alkali end members, with a deep minimum at a Na^+/K^+ molar ratio of 1:4 (2). This is known as the mixed alkali effect, which was first observed for alkali ion conductivity in glasses in the late 1960s (3). The conductivity decrease reflects the slowdown of diffusion of both mobile ions. The effect is detrimental not only for the rate but also for the selectivity of ionic transport. The mixed alkali effect occurs in the solid state only, and it is the immediate consequence of cation ordering, with the highest order at the composition of the minimum of the total conductivity (2). Selective ion transport, as discussed in this review, not only is a matter of ion mobility within a given material but also is affected by ion partitioning between ion conductor and its environment. A discussion of selective ion transport must therefore also specify the environment. Here, we consider only aqueous solutions that reversibly exchange ionic species (ions and their associates) with the ion conductor within the chemical stability range of both interacting phases.

Ideally, the ion conductor exchanges only one type of mobile ion with its environment. Examples include F^--conducting LaF_3-based solid electrolytes, which are inert in aqueous solutions containing a variety of ions. It is this selective exchange of F^- ions and the moderate ion conductivity that make Eu-doped LaF_3 suitable as separator material for F^--selective electrode (sensor) applications (4). For sensors, high selectivity is essential whereas ionic conductivity must be only high enough for transmitting the electrical signal. In fact, the F^- conductivity of Eu-doped LaF_3 is only in the range of microsiemens per centimeter.

For many technical high-current electrochemical applications (e.g., flow batteries, chlor-alkali electrolyzers, and electrochemical desalination cells), however, fast and selective transport of specific ions across separators is mandatory. For these applications, mostly ion exchange membranes (IEMs) are used, and the choice of a particular membrane type is a trade-off between membrane conductivity and selectivity (5, 6). IEMs are usually ionomers (a portmanteau of the words *ion* and *polymer*), that is, polymers with fixed ionic groups [e.g., $-SO_3^-$ and $-COO^-$ for cation exchange membranes (CEMs) and quaternized ammonium for anion exchange membranes (AEMs)]. Because the ionic groups are hygroscopic, such ionomers hydrate in the presence of water, and

because of the hydrophobic character of the polymer part, they phase-separate at the nanometer scale. The polymeric phase may even present some crystallinity (i.e., an ordered structure such as a crystalline solid), and the aqueous phase contains the counterions, which charge-compensate the charge of the fixed ionic groups. Immersed in aqueous solutions, the aqueous domain may not only reversibly exchange counterions but also take up other solutes, including ions with the same charge as the fixed ionic groups (co-ions). Conceptually speaking, the solid stationary polymeric part of ionomers provides them some structure (morphology), and the liquid aqueous ionic domains constitute the pathways for fast ionic transport. An interesting question then is whether the chemical and structural degrees of freedom of such hybrid systems allow for obtaining high and selective transport of a particular type of ion even when the membrane is in contact with many other kinds of species.

This review approaches this question in a systematic way by discussing partitioning of ions between ionomers and aqueous solutions and identifying parameters controlling ionic mobility within the ionomer. Before doing this, we commence with a prologue, drawing the reader's attention to ionic transport across biological membranes to help set the stage for this discussion. At the end of this review, we consider implications for the performance of IEMs in vanadium-redox-flow batteries (VRFBs) and present design strategies for membranes for this particular application. Nonetheless, the general insights provided in the main part of this review may also serve as a toolbox for optimizing IEMs for other applications requiring fast and selective ionic transport.

2. PROLOGUE

2.1. Achieving High Selectivity at the Expense of Conductivity: Selective Complexation by Ionophores

The selectivity of ion transport across biological membranes is mostly the consequence of the selective uptake of a particular type of ion. Whereas mixed ion ordering is detrimental for ionic conductivity and selectivity (see Section 1), the selective coordination or complexation of a specific kind of ion by ionophores (from the Greek *ion* and *–phore*, meaning "ion carrier") is key for obtaining selective, albeit slow, ionic transmembrane transport. This type of ion transport comprises the flux of charged ion–ionophore complexes with the usually more numerous neutral ionophores drifting in the opposite direction (**Figure 1*a***). The most prominent ionophore is valinomycin, a cyclodeca-depsipeptide produced by numerous kinds of streptomycetes (e.g., *Streptomyces fulvissimus*). Valinomycin is a natural antibiotic that forms stable complexes with potassium ions. The lipophilic character of the ionophore allows such complexes to enter and cross the lipid membrane of bacteria (**Figure 1*a***). In this way, they can transport K^+ out of the cell, depolarizing the resting potential across the cell membrane, which leads the cell to die. In the early 1960s, it was already known that depsipeptides can specifically affect alkali metal ion transport through biological (mitochondrial) membranes (7). Later, the group of Wilhelm Simon at ETH Zürich (8, 9) revealed the complexation of K^+ by valinomycin to be highly selective, with a complexation constant for K^+ that is approximately four orders of magnitude higher than that for Na^+ (in an aqueous environment). This discovery was possible because the group dissolved valinomycin in an artificial liquid membrane consisting of a polyvinyl chloride (PVC) matrix, a lipophilic membrane softener, and further additives. The formation of stable Nernst potentials across the membrane that correspond to different K^+ concentrations in aqueous solutions in contact with both sides of the membrane established K^+ transport across the membrane, and the low cross-sensitivity with respect to changes of the Na^+ concentration proved the high selectivity for K^+ transport over Na^+ transport. This was the birth of ion-selective electrodes using ionophores as ion carriers.

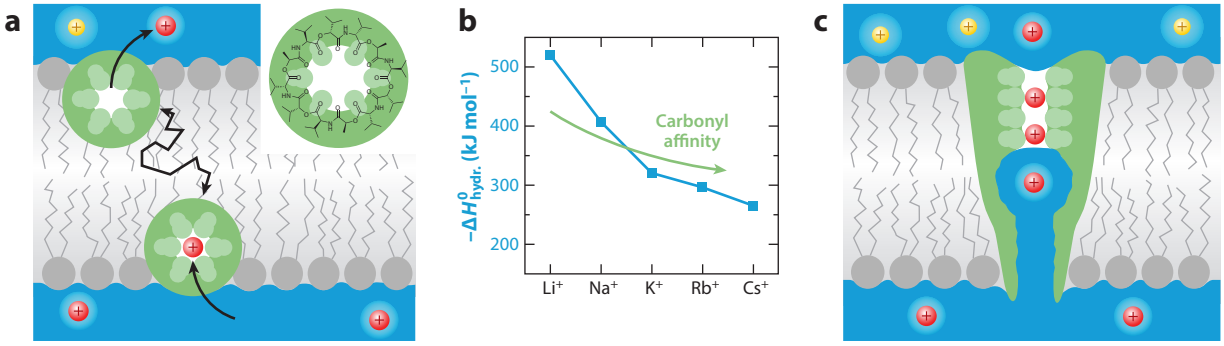

Figure 1

Ion transport through phospholipid membranes via ionophores and transmembrane proteins. (*a*) Molecular structure of the ionophore valinomycin with six carbonyl groups involved in K^+ (*red spheres*) coordination (13). Valinomycin dissolves in the lipophilic interior of the phospholipid membrane, where it acts as a mobile carrier for cross-membrane transport of K^+. Also, Na^+ (*yellow sphere*), with its larger hydration shell, is shown. (*b*) Absolute enthalpy of hydration of gaseous alkali metal ions and trend for the interaction energy of these ions with carbonyl groups. Note that the carbonyl has a pronounced negative inductive effect (−I) and the electronegativity of the alkali metal ions decreases from Li^+ to Cs^+. (*c*) Illustration of the structure of a K^+-conducting channel as revealed by MacKinnon and colleagues (20). Note that the narrow hydrophobic selectivity filter at the top has four sites where K^+ can localize by coordinating to eight carbonyl groups. Both ends of the selectivity filter are in contact with bulk water (*blue*).

Valinomycin is still used as an ion carrier in membranes of K^+-selective electrodes [a typical membrane composition is 33 wt% PVC, 65.8 wt% 2-nitrophenyl octyl ether, and 1.2 wt% of a mixture of valinomycin and potassium tetrakis(4-chorophenyl)borate of the molar ratio 2:1 (10)]. Ever since, the ETH group has developed many artificial ionophores with different selectivity profiles (for reviews, see 11, 12). Many of these are commercial, with "ETH" part of their acronym.

As expected from the large size of neutral ionophores and charged ionophore–ion complexes, both of which diffuse in the lipophilic liquid phase of ion-selective membranes, the conductivity of such membranes is rather low [typically in the microsiemens per centimeter range (10)]. What is making these systems fundamentally interesting, however, is the high selectivity of the formation of ion–ionophore complexes. The high K^+/Na^+ selectivity is usually explained by size constraints that physically prevent the valinomycin cavity (**Figure 1*a***) from collapsing onto the small sodium ion, whereas the larger potassium ion is well coordinated by 6 of the 12 carbonyl oxygens (13). A comprehensive literature on ion coordination in ionophores and ion-conducting channels (14) describes the conformational constraints on ion coordination and the effect they have on the total Gibbs energy of the system. Surprisingly, such approaches disregard the effects of specific chemical interactions, which vary greatly for different alkali metal ions in IEMs (15) (see Section 3.2). We therefore would like to emphasize the power of basic chemical concepts for explaining the selectivity of ion complexation through ionomers.

Here, the key issue is how the stabilizing effect of ion coordination within the cavity of the ionophore compares with the stabilizing effect of ion solvation in water. Ignoring the entropy change associated with ion coordination, the measure relevant to the aqueous environment is the heat of hydration. Water is a medium with a high static dielectric constant stemming from the large oscillator strength of the Debye relaxation, which is a collective process comprising reorientation of water dipoles and translational degrees of freedom such as the polarizability of protons within hydrogen bonds (Zundel polarizability) (16). The interaction of water with ions is therefore governed by electrostatics, which naturally explains the strongly increasing heat of hydration, with both increasing ion charge and decreasing ion size increasing electric field strength around the ion. For monovalent alkali metal ions, the heat of hydration is largest for Li^+ (−520 kJ mol^{-1}),

which is twice the hydration enthalpy of the hydrophobic Cs^+ (-264 kJ mol^{-1}) (**Figure 1*b***). The hydration process involves the formation of a stable hydration shell, which is largest for the small Li^+. This is why the smallest alkali ion has the largest hydrodynamic radius and the smallest diffusion coefficient in water. Of course, for the Na^+/K^+ pair the differences are smaller but still significant. For the K^+/Na^+ selectivity of valinomycin it is relevant that hydrated Na^+ is larger and more stable than hydrated K^+. To enter the valinomycin cavity, both ions have to strip off their hydration shell before coordinating with the carbonyl oxygens. One important point for understanding the selectivity of this process is that the underlying stabilizing interactions in this low dielectric environment change differently than they do for hydrated ions when moving from Na^+ to K^+. We hypothesize that the stabilizing effect involves significant electron transfer from the alkali metal ion to the carbonyl ligands. The carbonyl group has a pronounced negative inductive effect ($-$I) and the electronegativity of K^+ is lower than that of Na^+. The concept of electronegativity is usually used for elements, but there is no reason to not apply it to cations (see Section 3.2). We therefore expect some electron transfer from K^+ toward the carbonyl oxygen, making K^+ even more positive. Contrary to hydration, this stabilizing effect should increase from Li^+ to Cs^+, corresponding to the increasing electropositivity and polarizability of the ions. Consequently, the binding energy of alkali metal ion to carbonyl is anticipated to decrease less than the heat of ion hydration when moving from Li^+ to Cs^+ (**Figure 1*b***). A molecular dynamics simulation found similar trends for the free energy by considering only electrostatic properties of carbonyl ligands (17).

In consideration of this, one expects the driving force for alkali metal ions to transfer from an aqueous environment to the cavity of valinomycin in order to continuously increase from Li^+ to Cs^+. The surprising observation that valinomycin-based selective electrodes are even more sensitive toward the larger Rb^+ and only slightly less selective toward Cs^+ (18) supports this simple chemical rationale. It does not seem to be the ion size but rather how the different chemical interactions correlate with size (**Figure 1*b***) that decides whether an alkali metal ion prefers an aqueous environment or the electron-withdrawing cavity of valinomycin.

2.2. Combining High Selectivity and High Ionic Fluxes Through a Sophisticated Device: The Case of Ion-Conducting Channels

Fast and selective K^+ conductivity across cell membranes is key to essential biological processes such as muscle cell contraction, nerve excitation, and hormone secretion (19). Although chemically related to that of ionophores, the conduction mechanism of transmembrane ion-conducting channels is fundamentally different. These channels are formed by proteins spanning the entire phospholipid membrane (approximately 3.4 nm), but the part providing the channel with its selectivity, the selectivity filter, is only 1.2 nm long (**Figure 1*c***). MacKinnon and colleagues (20) first revealed this in 1998 with an X-ray diffraction study of crystallized potassium channels from *Streptomyces lividans*. As in valinomycin, the potassium ion coordinates to carbonyl groups of the proteins' backbone, pointing toward the center of the channel. The potassium coordination number is higher in the channel than in valinomycin (8 instead of 6), and there are four binding sites, two of which are occupied by K^+. The authors state that the binding mimics the stabilizing effect of K^+ hydration and that structural constraints keep the selectivity filter open to coordinate K^+ ions but not smaller Na^+ ions. This idea is related to the explanation of size constraints affecting the selectivity of K^+/Na^+ complexation by valinomycin (see Section 2.1).

Bearing in mind the above considerations of K^+ binding to the ionophore valinomycin, we suggest that the stronger interaction of Na^+ with water molecules than with carbonyl groups may

be the primary reason for the highly selective K^+ uptake (**Figure 1*b***). Then, it is not the ion size per se but the related electrostatic and electronic properties that make the difference.

This idea is supported by the observations that some K^+ channels are more selective for Rb^+ and Cs^+ (21–24) and that the conduction of these larger ions is also less efficient. Both observations could be natural consequences of stronger binding of these ions in the filter than in the aqueous phase (**Figure 1*b***). Electrostatics alone already predicts the principal trends: For ligands with low electrostatic field strength (such as carbonyl), the stabilization through carbonyl coordination compared with hydration increases from Li^+ to Cs^+. These are the two end members of one of the Eisenman sequences, which describe alkali metal ion binding to ligands of different field strength (25, 26). They were used to explain ion selectivity of biological channels long before the first structural information was available. The importance of specific interactions compared with those of steric effects is also underlined by the chemically different nature of Na^+ channels. These are not simply narrower versions of K^+ channels lined with hydrophobic electronegative carbonyl groups. Their interior is more hydrophilic, for example, with negatively charged glutamic acid residues interacting with partially hydrated Na^+ (27).

In Section 3.2, we discuss related observations for IEMs in terms of ion partitioning and ion mobility. Here, the stabilization of K^+ in the filter of ion-conducting channels, compared with its stabilization in the aqueous phase, seems to be strong enough for entering the filter but not too strong so as to immobilize the ions.

This leads us to the issue of ion mobility in the filter. The high selectivity of K^+ uptake over Na^+ uptake prevents the presence of different types of ions and, with this, ion ordering and retardation within the filter, similar to the mixed alkali effect in β'' alumina (see Section 1). The short (1.2 nm) selectivity filter is in contact with bulk water not only at the end pointing toward the extracellular side but also at the end pointing toward the center of the membrane, where structural analysis (20) revealed a water-filled cavity (pool) with a diameter of ~1 nm (**Figure 1*c***). This is approximately the size at which water assumes bulk properties, including its typical high dielectric constant. Therefore, K^+ is equally stabilized through hydration on both sides of the selectivity filter. This symmetry reduces the width of the activation barrier of ion migration to the length of the short selectivity filter. In contrast to the contacting water, the filter has a low dielectric constant and no negative ionic groups, which could compensate the charge of entering cations. Apart from the stabilizing interaction through the coordination with the negative carbonyl oxygens, electrostatics therefore progressively destabilizes the system the more K^+ moves toward the center of the selectivity filter. This has already been recognized by the MacKinnon group, and they suggested that the electrostatic repulsion between the two K^+ ions within the filter lowers the energy penalty for ion migration. One may even speculate that the two K^+ ions still have a residual polarizing effect on the neighboring water pools and that this stabilizing interaction decreases for one K^+ ion while increasing for the other ion when both move through the filter in a cooperative way. Also, this is expected to have a reducing effect on the global energy barrier. The throughput rate of K^+ is 10^8 ions per second (20), which is commonly considered to be close to the diffusion limit (24). In fact, with a diffusion length of 1.2 nm, a diffusion coefficient of $\sim 10^{-10}$ m^2 s^{-1} is only 20 times lower than the diffusion coefficient of K^+ in bulk water, even though the nature of this diffusion is different from that in water. The directional and cooperative dynamics allows for efficient diffusion even at low jump rates (note that typical jump rates in bulk water are in the 10^{11} s^{-1} range).

Following the above discussion, the combination of fast and selective K^+ transport through potassium channels seems to be the consequence of (*a*) similar stabilization energies for K^+ coordinating with water in the aqueous phase and carbonyl ligands within the dry channel filter, (*b*) the

coupled directional translocation of two ions, and (*c*) the short length of the dry selectivity filter (1.2 nm), which is in contact with bulk water on both sides.

Rapid K^+ exchange with the aqueous phase for the K^+–valinomycin complex is also observed. In this respect, there is even some similarity between ionophores and ion-conducting channels (28).

3. SELECTIVE ION TRANSPORT THROUGH ION EXCHANGE MEMBRANES

The above examples show that relations between ion transport and selectivity are usually complex, and the mechanisms leading to transport and allowing for some selectivity appear to depend on the particular system. Nevertheless, the parameters describing these processes are similar for the different cases. Because we are dealing with ionic transport, it is not surprising that electrostatics is always involved, specific chemical interactions may play diverse roles, and morphology (structure) is an important ingredient of ion–host interaction. Although these are not clear-cut categories, we use them for a systematic discussion of ion partitioning and ion mobility in IEMs.

Figure 2 illustrates the two situations we consider: the phase-separated morphology of an IEM with the polymer domain and the aqueous ionic domain in contact with aqueous solutions of low and high ionic strength. The fixed ionic groups are covalently connected to the polymeric structure and localize at the inner surface separating the two domains. In dilute solutions, the charge of the fixed ions is compensated by the opposite charge of the counterions, which may either bind to the fixed ions or stabilize in the interior of the aqueous domain, where they are mobile. As long as the ionic strength of the external solution is lower than the ionic strength within the hydrated membranes, co-ions are prevented from entering the membrane [the Donnan exclusion effect (29)]. However, counterions may still exchange with ions of the same charge sign in the solution. When the ionic strength of the aqueous solution in contact with the membrane is not small compared with the ionic strength of the membrane interior, co-ions together with

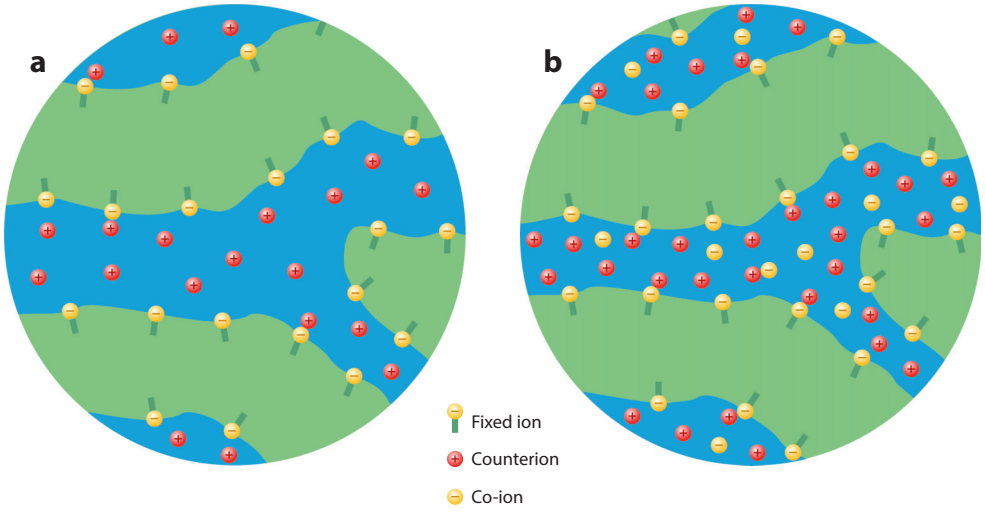

Figure 2

Illustration of nanophase-separated morphology of ion exchange membranes in contact with aqueous solutions of (*a*) low and (*b*) high ionic strength. Fixed ionic groups (*yellow spheres*) localize at the inner interface separating the polymeric phase (*green*) and aqueous ionic phase (*blue*) (15).

an equivalent number of counterions enter the membrane interior (i.e., the breakdown of the Donnan exclusion effect).

The Donnan picture considers electrostatics as the only type of interaction. (Species are characterized only by their charge and concentration and by whether their position in space is fixed.) The following discussion on ion partitioning and ion mobility also includes the effects of chemical interactions (Section 3.2) and morphology (Section 3.3) accounting for incomplete dissociation and steric restrictions of diffusional processes.

3.1. Electroselectivity

The original work of Donnan (29) deals with ion partitioning between charged polymers and aqueous electrolytes, and it was soon recognized that this has immediate implications for ionic permeation [*perméabilité ionique* (30, 31)]. The most obvious consequence of Donnan exclusion is that CEMs preferentially conduct cations and AEMs preferentially conduct anions, but also the ions' valence state (z) affects selectivity of ionic transport through membranes bearing fixed ionic groups. For such purely electrostatic effects, the term electroselectivity (*Elektroselektivität*) has been used since the 1950s (32). Because the equivalent conductivity of different ions in ionomers (33) falls into a narrow range [similar to the situation for aqueous solution (34)], the partial conductivities (transference numbers) of ions in IEMs are closely related to their respective concentrations (equivalents). This is true as long as there is no ion association, including Manning's counterion condensation (35), and no morphological restrictions to ion mobility. The governing equations are then simple. For all mobile species i, which exchange between the external solution and the membrane (denoted by superscript sol and mem, respectively), the electrochemical potentials η_i are equal for both phases:

$$\eta_i^{\mathrm{sol}} = \eta_i^{\mathrm{mem}}, \qquad 1.$$

$$\mu_i^0 + RT\ln(\gamma_i^{\mathrm{sol}} \cdot m_i^{\mathrm{sol}}) + z_i F\varphi^{\mathrm{sol}} = \mu_i^0 + v_i(p^{\mathrm{mem}} - p^0) + RT\ln(\gamma_i^{\mathrm{mem}} \cdot m_i^{\mathrm{mem}}) + z_i F\varphi^{\mathrm{mem}},$$

where m_i is the molalities, γ_i is the activity coefficients and the Donnan potential is the electrostatic potential difference $\varphi_{\mathrm{Donnan}} = \varphi^{\mathrm{mem}} - \varphi^{\mathrm{sol}}$.

Equation 1 also applies to neutral species such as H_2O ($z = 0$). The term $v_i(p^{\mathrm{mem}} - p^0)$ (where v_i is the molar volume) describes the increase of chemical potentials with pressure p^{mem}, which may be included for membranes sustaining high swelling pressures (36).

The electroneutrality condition,

$$z_{\mathrm{counter}} m_{\mathrm{counter}}^{\mathrm{mem}} = z_{\mathrm{fixed}} m_{\mathrm{fixed}} + z_{\mathrm{co}} m_{\mathrm{co}}^{\mathrm{mem}}, \qquad 2.$$

then completes the set of equations (the subscripts counter, fixed, and co refer to counterion, fixed ion, and co-ion). Note that for the membrane this condition also contains the charge stemming from the fixed ionic groups.

In the next section, we discuss solutions of such sets of equations for a given concentration of fixed ionic groups (m_{fixed}) or fixed water content expressed as hydration number $\lambda = [H_2O]/[\text{fixed ion}]$.

3.1.1. Cation/anion selectivity. In pure water, an AEM conducts anions and a CEM conducts cations. These mobile ions are counterions and are confined to the system only through the electroneutrality condition (**Figure 2**; Equation 2). The huge chemical potential difference $\Delta\mu_i$ of these ions for the membrane and for the external water is then compensated for by a corresponding electrostatic potential difference $\varphi_{\mathrm{Donnan}}$. In the case of a CEM, this potential is negative

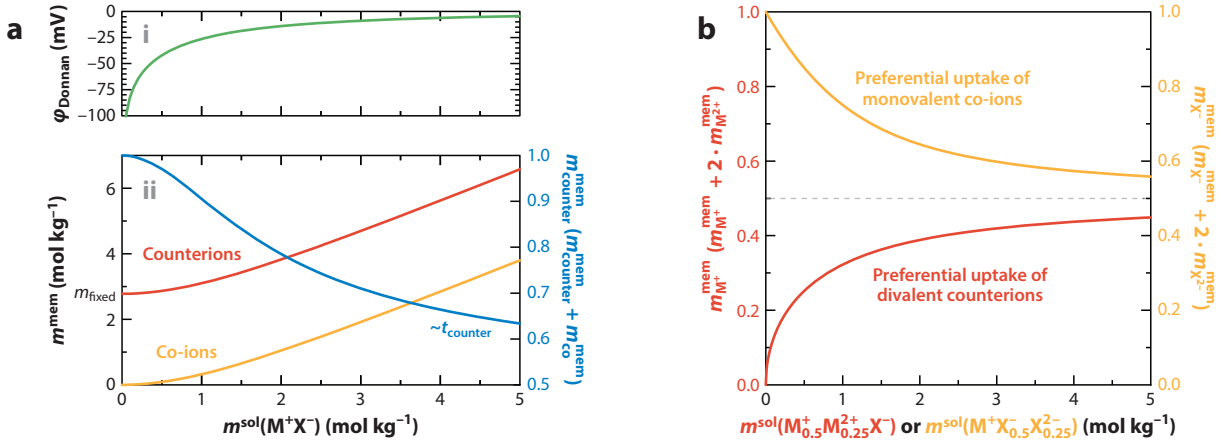

Figure 3

(*a*) Ion partitioning between a 1:1 electrolyte and a membrane with a water content of $\lambda = 20$ corresponding to $m_{fixed} = 2.78$ mol kg^{-1}. (*i*) The electrostatic potential difference φ_{Donnan} between membrane and solution. (*ii*) Co-ion and counterion uptake as a function of electrolyte concentration, and the mole fraction of counterions as an estimate for the counterion transference number $t_{counter}$. (*b*) Partitioning of monovalent and divalent ions in contact with a solution with an equal number of both ions. For counterions (constituting the majority of mobile ions) divalent ions are preferentially taken up (*bottom*), whereas the opposite is true for co-ions (*top*). Note that both functions are not symmetrical.

(**Figure 3*a***, **subpanel *i***) with respect to the solution because the chemical potential gradient of cations is driving them out of the membrane and separating them from the negative fixed ionic groups until electrochemical equilibrium is established.

In the presence of exchangeable ions in the aqueous environment, however, both co-ions and counterions enter the membrane in equal amounts (again, because of electroneutrality), and the electrostatic potential difference decays. Solving the above general set of equations for this simple case (assuming γ_i to be identical in solution and membrane and neglecting pressure terms) then yields the well-known Donnan equation for co-ion uptake m_{co}^{mem} as a function of the concentration (molality) of an external 1:1 electrolyte solution m^{sol}:

$$m_{co}^{mem} = \frac{1}{2}\left(\sqrt{(m_{fixed})^2 + 4 \cdot (m^{sol})^2} - m_{fixed}\right). \quad 3.$$

This, together with the fraction of mobile counterions (total concentration of mobile ions in the membrane is taken as reference), which is a good estimate for the transference number t_+ of cations (see above), is shown in **Figure 3*a***, **subpanel *ii***. This measure of selective counterion (cation) transport decreases with increasing salt concentration in the surrounding solution, reaching a value of $t_{counter} \sim 0.9$, for a 1 m solution. For high salt concentrations (such as in flow batteries), IEMs almost lose their cation/anion selectivity; that is, their transport properties approach those of simple (uncharged) diaphragms. However, their high selectivity in dilute solutions is extensively exploited in applications such as reverse osmosis (5).

3.1.2. Discriminating between different valence states. Another interesting issue is partitioning of ions of different valence states. Here, we consider two cases of IEMs with monovalent fixed ionic groups equilibrated in salt solutions with (*a*) equal numbers of monovalent and divalent counterions and (*b*) equal numbers of monovalent and divalent co-ions. The above set of equations has been solved for both cases (see the **Supplemental Material**).

Supplemental Material >

If, for example, a CEM is in contact with a dilute solution with equal numbers of monovalent and divalent cations, the membrane selectively takes up divalent counterions. The reason is simply because this minimizes the concentration gradient (chemical potential difference) of mobile cations between the membrane and the solution and the corresponding Donnan-potential difference (φ_{Donnan}). With increasing salt concentration in the solution, however, co-ions (anions) (see Section 3.1.1) together with an equal number of cations also enter the membrane, and the concentration ratio of monovalent to divalent cations approaches that of the external solution (see the bottom of **Figure 3*b***).

The other case is that of monovalent and divalent co-ions in the solution. For CEMs, this would be anions of different valence state. The electrostatic driving force $zF\varphi$ for these co-ions is then opposite of the driving force for the counterions, and this is higher for divalent than for monovalent co-ions (anions). Therefore, the membrane selectively takes up monovalent anions from dilute solutions (see the top of **Figure 3*b***). Of course, the fraction of mobile anions (co-ions) in the membrane is small (the membrane is still a predominant cationic conductor), and the decay of this selectivity with increasing salt concentration of the solution is less pronounced than for the discrimination of counterions with a different charge (see the bottom of **Figure 3*b***).

The implications for the separation of ions with different valence states [e.g., separation of Li^+ and Mg^{2+} by electrodialysis (5)] are not straightforward, because the fractions of ions with different valence states in the membrane are also functions of current density and boundary conditions. For example, a CEM preferentially contains and conducts divalent cations rather than monovalent cations in dilute solutions only for low current density. With increasing current density, divalent cations progressively deplete in a near-surface layer of the contacting solution at the anode side. This depletion process is the consequence not only of the preferential transport of divalent cations by the ionic current but also of the less efficient transport of divalent cations from the bulk of the solution into the near-surface layer, which is a diffusional process (5, 37). Note that equivalent conductivities of divalent and monovalent ions in aqueous solutions are usually similar (34), but (tracer) diffusion coefficients are different by a factor of ~2. (The more extended and more robust hydration shells of higher-valence ions generally reduce their diffusion coefficient in water.) Because of this, an increasing fraction of monovalent cations incorporate and conduct in the membrane.

Instead of suppressing this effect, it may even be enhanced for, for example, making a CEM selective for the transport of monovalent cations in the presence of divalent cations in the solution. This can be achieved by coating the anode side of the CEM with a thin layer of an AEM. For an AEM, cations are co-ions that are taken up in small concentration but with a high preference for monovalent cations (see the top of **Figure 3*b***). Hence, the thin AEM serves as a blocking layer for divalent cations (5). CEMs coated with a thin layer of an AEM increase the monovalent ion selectivity of membranes used in reverse electrodialysis (38). In the highly acidic environment of VRFBs, basic polybenzimidazole (PBI) coatings have been used for suppressing multivalent vanadyl cation transport (39). Here, the idea is that protonation of PBI's basic sites makes this polymer an AEM rejecting higher-valence cations, but the rejection of large vanadyl cations is most likely also a morphological effect (see Section 3.4). Higher-valence-cation rejection is also achieved by coating CEMs with a thin polycation layer (40) or a layer-by-layer assembly of polycations and polyanions with polycation termination (41, 42). Even nanofiltration membranes coated with such multilayers show good selectivity for the transport of monovalent cations (43), suggesting that multilayers alone may explain the selectivity. The reason for this may be a combination of size exclusion (see Section 3.3) and electroselectivity (Donnan exclusion) (43). Of course, the concept is also applicable to AEMs: An AEM coated with a thin polyanion layer demonstrated an increased selectivity for the transport of monovalent anions than of divalent anions (44).

3.2. Effects of Specific Interactions

In Section 2 we suggest that specific (chemical) interaction of mobile ions with their environment affects selectivity and transport relations in different ways. Stable ion complexation through carbonyl ligands of ionophores forms hydrophobic ionic charge carriers that dissolve in the hydrophobic interior of phospholipid membranes, where they are mobile (**Figure 1*a***). The same type of interaction has to balance ion hydration for entering the dry selectivity filter of ion-conducting channels without trapping the ion (**Figure 1*c***). In IEMs, however, transport takes place in the aqueous ionic phase. Here, mobile ions interact mostly with fixed ionic groups, and these types of interactions are similar to the relevant interactions in ionophores and ion-conducting channels. The way these interactions affect selectivity transport relations, however, adds another facet to the role of specific interactions.

For instance, in AEMs with quaternized ammonium (QA^+) as a fixed ionic group, such groups may form stable associates with mobile ions (e.g., $[QA - Cl - QA]^+$) (45). This reduces conductivity because ion association leads to a reduction of the membrane's water content. But even for identical water content, conductivity is reduced in the presence of ion association. In fact, it was the conductivity reduction that had first pointed toward an immobilization effect, and it was later shown that this also affects ion partitioning.

Preferential uptake of one type of ion over another is a long-known phenomenon for CEMs [especially Nafion (46)]. This was initially described with selectivity coefficients, implicitly assuming uniform chemical environments of the respective ions (one-state model) not only in solution but also within the membrane.

The first modeling attempts by Pintauro and colleagues (47, 48) were of this sort. They modeled the effect that fixed ions have on the orientation of water and how this affects the solvation of the diverse counterions. Their model found that the dielectric constant of water is reduced close to the water–polymer interface and is maximum in the middle of the aqueous domains. Consequently, ions with high hydration enthalpy localize in the bulk of the aqueous domains and ions with low hydration enthalpy localize closer to the water–polymer interface (see also **Figure 1*b***). These purely electrostatic considerations alone yield the right trends with respect to partitioning of Li^+ and Cs^+ between aqueous solutions and Nafion, where they are counterions. This group considers only divalent counterions for the formation of coordinate covalent bonds (49). Later, Okada et al. (50) measured partitioning of other pairs of ions, and they were the first to find that the selective uptake of a particular type of ion does not noticeably affect its transference number (compared with the transference number of the contacting aqueous solution).

Our own recent work not only proves the empirical finding of Okada et al. but also provides a rational, consistent explanation for ion partitioning and ion transference numbers by ion association with fixed ionic groups (15). Two important results of this work are that two chemically distinct states (ions are either associated and immobile or dissociated and mobile) describe ion partitioning quantitatively and that the interactions governing mobile ions' association with fixed ionic groups receive significant contributions from specific chemical interactions (beyond electrostatics).

In addition, Li^+ and Cs^+ were chosen pars pro toto for our work not only because they are the two alkali metal ions with the most extreme properties (see also **Figure 1*b***) but also because their isotopes, ^7Li and ^{133}Cs, are suitable for nuclear magnetic resonance (NMR). In fact, on the NMR timescale two distinct populations (mobile and immobile) are clearly identified for both types of ions, and from their ratios of incidence the dissociation constant K_I ($I = Li^+, Cs^+$) for each ion type is obtained. With this empirical information and measured membrane water content λ, Li^+/Cs^+ partitioning between aqueous solutions and Nafion as calculated without any adjustable

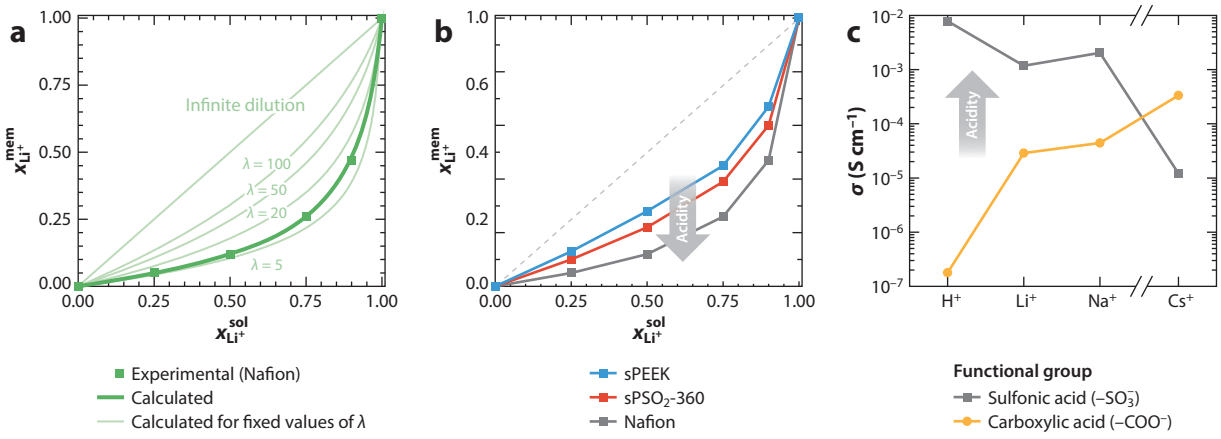

Figure 4

(*a*,*b*) Li^+/Cs^+ partitioning between aqueous solution and cation exchange membranes (note that $x_{Li^+} = 1 - x_{Cs^+}$). (*a*) Experimental data for a Nafion membrane and calculated data using experimental values for K_{Li^+}, K_{Cs^+}, and λ (ranging from 7 to 18 for Cs^+- and Li^+-rich Nafion) (15). Calculated data for different fixed values of λ predict that selective uptake of Cs^+ over Li^+ progressively diminishes with increasing membrane hydration. (*b*) Li^+/Cs^+ partitioning between aqueous solution and ionomer membranes with sulfonic ionic groups of different acidity: random sPEEK (*IEC* = 1.5 meq g^{-1}), $sPSO_2$ (*IEC* = 4.55 meq g^{-1}), and Nafion (long-side-chain PFSA with an *IEC* of 0.94 meq g^{-1}). (*c*) Room-temperature H^+, Li^+, Na^+, and Cs^+ conductivity of perfluorinated ionomers with sulfonic and carboxylic fixed ionic groups for a fixed hydration number (λ = 6) (52). Abbreviations: *IEC*, ion exchange capacity; mem, membrane; PFSA, perfluorinated sulfonic acid; sol, solution; sPEEK, sulfonated poly(ether ether ketone); $sPSO_2$, sulfonated poly(phenylene sulfone).

parameter perfectly matches the experimental data (**Figure 4*a***). With the given values for K_I, ion partitioning is also calculated for any water content λ, and as expected from the nature of the given model, selectivity is progressively lost with increasing λ, that is, with progressive dissociation of both ionic species (**Figure 4*a***).

To understand the degree of dissociation of different types of ions, we have to compare the stabilizing effects through ion hydration with the stabilization through specific interactions of the ion with the fixed ionic group, as we did for carbonyl coordination in biological systems (see Section 2). Surprisingly, selectivity of ion uptake does not depend on the membrane's ion exchange capacity (*IEC*), but it very much depends on slight changes to the chemical character of the fixed ionic group (15). For ion uptake of ionomers with sulfonic fixed ionic groups, the Cs^+/Li^+ preference markedly increases with increasing acidity of the sulfonic group (**Figure 4*b***). For the given examples, the Brønsted acidity is affected by the chemical influence of the polymer to which the ionic group is attached. The perfluorinated sulfonic acid (PFSA) Nafion is a superacid that shows not only the most pronounced Cs^+/Li^+ selectivity but also the lowest degree of dissociation for both ions. This seems counterintuitive considering the lower negative charge density on the conjugated base ($-SO_3^-$), which is expected to reduce the electrostatic attraction with cations. However, the reduced electric field strength around the fixed ionic group also reduces the interaction with hydration water, therefore favoring ion association. This effect is part of the electrostatic model developed by Eisenman & Horn (26), which partially explains the increasing cation association with increasing Brønsted acidity. Such types of models, however, treat ions as charged hard spheres, which is a severe simplification especially for large cations such as Cs^+. The Brønsted acidity increase of Nafion goes along with not only a decreased negative charge density but also an increased electronegativity of its conjugated base ($-SO_3^-$), creating a driving force for electron transfer from the highly polarizable Cs^+ toward the fixed ionic group that leads to some coordinate

covalent bonding (15). Compared with Li^+, Cs^+ not only has a lower field strength and therefore a lower hydration enthalpy (see also **Figure 1*b***) but also is electronically much more polarizable [3.34 $Å^3$ for Cs^+ compared with 0.03 $Å^3$ for Li^+ (51)] and has a lower electronegativity. Consequently, Cs^+ binds strongly to the conjugated base of strong Brønsted acids and Li^+ is stabilized in the aqueous phase through hydration. As expected, the trend is inverted for alkaline metal ion association with weakly acidic fixed ionic groups. The conductivity of perfluorinated ionomers of similar *IEC* and fixed water content ($\lambda = 6$) strongly increases when moving from H^+ to Li^+ to Na^+ to Cs^+ as counterions for carboxylic fixed ionic groups ($-COO^-$) and decreases for sulfonic fixed ionic groups ($-SO_3^-$) (52) (**Figure 4*c***). For the weak Brønsted acid –COOH, the effective negative charge of its conjugated base ($-COO^-$) is significantly higher and its electronegativity lower compared with those for sulfonic fixed ionic groups. In an aqueous environment, this leads to a stronger association of small and hard cations (such as H^+ and Li^+) and a weaker association of large and soft ions (such as Cs^+).

The effects of ion association on the selectivity of ion transport (transference numbers) were determined by measuring ^7Li and ^{133}Cs diffusion coefficients and by direct electrochemical transference (15). The applied NMR techniques provided averaged diffusion coefficients for both kinds of ions. These diffusion coefficients expectedly decrease with increasing degree of association. The interesting finding that the decrease is just by a fraction identical to the fraction of associated ions $x_{\text{associated}}$,

$$D_{\text{average}} = D_{\text{mobile}}(1 - x_{\text{associated}}), \qquad 4.$$

directly implies that the total conductivity decreases and that the transference numbers do not change regardless to what extent the ions are associated. The last conclusion holds only because the molar ratio of mobile ions in the membrane resembles that of the surrounding dilute solution.

This simple picture consistently supports the two-state model (see above). The immobilized (associated) ions are then taken out of thermodynamic equilibrium, the concentration of fixed ionic groups is reduced by neutralization (53), and there is no selective ion uptake when considering only mobile ions in the membrane. The last aspect is strictly true only for identical ion concentrations in the aqueous phase of the membrane, that is, for identical activity coefficients of mobile ions in the membrane and the solution (see below). This finding implies that the introduction of chemically active groups into the ionomer structure for binding a specific type of ion does not reduce the transference number of this particular ion type. We therefore assume that the improved VRFB performance of membranes containing pyridine functionalities for binding vanadium species is not only the consequence of vanadium binding as suggested by Gubler and colleagues (54).

All these results and considerations apply to membranes in thermodynamic equilibrium with dilute solutions. Specific interactions not only govern counterion partitioning but also affect co-ion uptake in concentrated solutions and, with that, counterion/co-ion (cation/anion) selectivity. However, even in the presence of such interactions, the Donnan equation (**Figure 3*a***, **subpanel *ii***; Equation 3) is perfectly valid provided the input data are adequately corrected. Specifically, (*a*) the concentration of fixed ionic groups must be reduced by the fraction involved in counterion association (53), and (*b*) in the case of strong ion hydration, the water of hydration must thermodynamically be allotted to the ion rather than to the water. The consequences are as obvious as they are striking. Association of a specific counterion (e.g., Cs^+ in PFSAs) may reduce the charge of IEMs to such an extent ($m_{\text{fixed}} \sim 0$) that any counterion conductivity or Donnan exclusion (cation/anion selectivity) is suppressed. Under these conditions, any IEM (CEM and AEM) behaves like a simple nanoporous diaphragm (15) for which transport of ions and other species is chiefly controlled by morphological features (see Section 3.3). Strong ion hydration, which is the case for Li^+, has the opposite effect. Because ionic strength is higher in the membrane than in the

surrounding solution, the relative increase of ion concentration through ion hydration is higher in the membrane than in the solution. As for the activity coefficients (γ) of all species dissolved in the aqueous ionic domain, their relative increase through hydration (55) is larger for the membrane than for the solution. For a given nominal water content, this leads to an increase of the Donnan exclusion effect (i.e., reduced co-ion uptake and enhanced cation/anion selectivity) (15). We speculate that exothermal hydration of the ionomer backbone leads to the same effects.

3.3. Morphological Effects

Thus far, we have deliberately excluded morphological effects by considering relatively small ions in well-swollen IEMs. For larger ions or other dissolved species within ionomers with narrow aqueous ionic domains, however, steric effects on ion mobility may emerge.

Such effects, occurring for molecular transport through the open, well-defined structures of zeolites, are well known (56). For technical zeolites, the term molecular sieve refers to the observation that molecular diffusion coefficients are high provided the molecule is smaller than the morphological bottleneck along the diffusion pathway. Later, such sieving effects were also demonstrated for the mobility of ionic species (57), and zeolite membranes have been used in VRFB applications for rejecting large electrochemically active vanadium species (58). More recently, ion sieving effects were observed for layered materials such as graphene oxide (59, 60), graphene oxide frameworks (61), and MXenes (62). That nanofiltration membranes perform well in VRFBs (63) and that polymeric nanoporous membrane coatings improve performance for this application (64, 65) qualitatively demonstrate ion sieving also for this type of porous polymer.

As for such uncharged polymeric materials, the structure (morphology) of most IEMs is ill-defined; hence, reported transport-morphology relationships are to date qualitative at best (66). The IEM with the most distinct morphology is prototypical Nafion. We could show that its morphology is locally flat, and we established a straightforward way to access the width of the aqueous ionic domain from small angle X-ray scattering (SAXS) data (67). With these data, we revealed quantitative relations between this morphological feature and the diffusion and mobility of ionic species in Nafion (68). We measured the diffusion coefficients of a small species and a large species in the same sample at different water contents. Because diffusion coefficients strongly depend on water content (especially when water content is low), and experimental data of water contents are usually flawed with large errors, only measurements of identical samples yield high accuracy for ratios of diffusion coefficients. **Figure 5*a*** shows the diffusion coefficients of a large cation [tetrakis(hydroxymethyl)phosphonium] and water in Nafion as a function of the water volume fraction Φ_{aq} as well as data for a dilute aqueous solution ($\Phi_{aq} = 1$). From the latter data, the hydrodynamic diameter of the phosphonium is calculated to be 0.62 nm, which coincides with the geometric extension of this cation. The diffusion coefficient of neutral water stands for the mobility of hydronium ions (H_3O^+), which is close to the water diffusion coefficient (33). The choice of a neutral species also avoids mixed ion effects (see Section 1 for the mixed alkali effect), which are small in liquids but may still introduce further complications. At high water content, the diffusion coefficients of both species are similarly affected by the reduction of the water content (i.e., the narrowing of the aqueous domain). Although this is mostly a long-range percolation effect resulting from increased tortuosity, the sharper decrease in diffusion coefficient recorded for phosphonium compared with water diffusion at low water content indicates a blocking effect on a local scale. This is clearly visible in the ratio between the two diffusion coefficients as a function of the width of the aqueous ionic domain d_{aq}. Such a ratio diverges when approaching $d_{aq} = 0.62$ nm (**Figure 5*b***) [i.e., the geometric extension of tetrakis(hydroxymethyl)phosphonium]. At the corresponding water content ($\lambda \sim 3$) the diffusion of phosphonium cations comes to a standstill whereas water (hydronium) still shows reasonable diffusion.

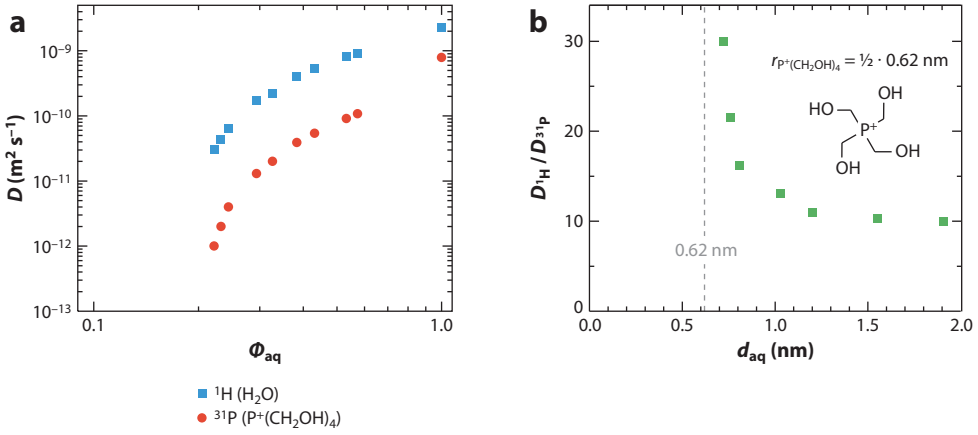

Figure 5

Diffusion coefficients of water and tetrakis(hydroxymethyl)phosphonium in Nafion as (*a*) a function of water volume fraction Φ_{aq} and as (*b*) a ratio of both diffusion coefficients as a function of the width of the aqueous ionic domain d_{aq} (*dashed line*) (68). The increase of this ratio for d_{aq} close to the extension of the phosphonium cation (0.62 nm, *dashed line*) is most likely an effect of size discrimination (sieving).

As we show in Section 3.4, this size discrimination (sieving) is even more pronounced for ions with a larger size difference and for ionomers with better-defined morphology.

3.4. Membranes for Redox-Flow Batteries

Redox-flow batteries are among the technologies that provide the potentially lowest cost of stationary electrical energy storage per unit installed capacity (69). This is mainly the result of their potentially large lifetimes (more than 10^4 cycles). In such batteries, ion-conducting membranes have to efficiently separate the electrochemically active ionic species (usually dissolved in 2–5 M of sulfuric acid) while conducting other ionic species (in most cases protons) for mediating the electrochemical reactions at a sufficiently high rate. The feasibility of the diverse types of redox-flow batteries therefore highly depends on the availability of separator membranes with high ionic conductivity and an appropriate selectivity profile. The latter mainly controls the battery's lifetime, which is still critical for most types of redox-flow batteries (70). An important exception to this behavior is observed in the all-VRFB, the most technically advanced system. The reason for this exception is that both electrolytes of VRFBs contain vanadium ions as redox-active species (V^{2+}_{aq} and V^{3+}_{aq} in the anolyte and VO^{2+}_{aq} and VO^{+}_{2aq} in the catholyte). Hence, any vanadium transport through the membrane reduces Coulomb efficiency (the ratio of integrated charges flowing during discharging and charging), but it does not lead to irreversible mutual chemical contamination of anolyte and catholyte. This is why VRFB operates reasonably well even with simple porous glass separators (71). A less obvious reason becomes apparent when considering the influence of ion partitioning, ion conductivity, and VRFB performance data (68). The vanadium uptake of a Nafion membrane equilibrated with a dilute solution of a model electrolyte (0.05 M $VOSO_4$, 0.05 M H_2SO_4) is hardly detectable (68). Under these conditions, Donnan exclusion is effective, and the membrane exchanges only cations (counterions) with the solutions. The fact that Nafion remains in its pure proton form therefore suggests that the VO^{2+} concentration in the electrolyte is small. Indeed, aqueous solutions of $VOSO_4$ behave as weak electrolytes (72), and VO^{2+} is present mostly as neutral $VOSO_4$ (the degree of dissociation of a 1.6 M $VOSO_4$ is lower than 5% and

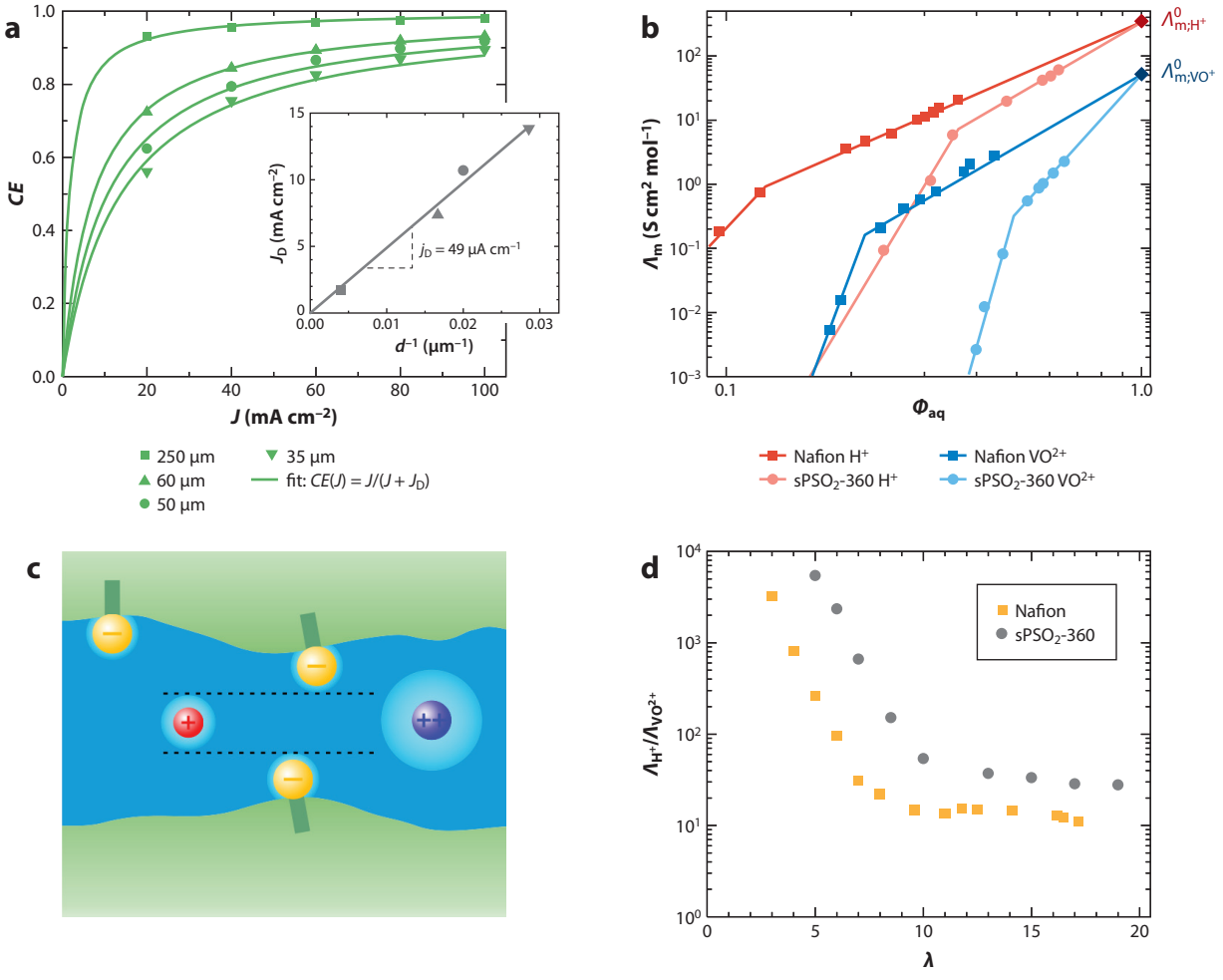

Figure 6

Vanadium transport through $sPSO_2$-360 (*IEC* = 2.7 meq g^{-1}) and Nafion. (*a*) Current-dependent Coulomb efficiency *CE(J)* of a VRFB with $sPSO_2$-360 membranes of various thicknesses including fits using Equation 5. The inset shows J_D as a function of d^{-1}, with a slope corresponding to the specific vanadium crossover current density j_D (68). (*b*) Equivalent conductivity Λ of proton and VO^{2+} as a function of water volume fraction Φ_{aq}. (*c*) Illustration of a morphological bottleneck at the onset of selectivity increase. (*d*) Ratio $\Lambda_{H^+}/\Lambda_{VO^{2+}}$ as a function of the hydration number λ. Abbreviations: *IEC*, ion exchange capacity; $sPSO_2$, sulfonated poly(phenylene sulfone); VRFB, vanadium-redox-flow battery.

the addition of sulfuric acid is expected to further decrease this number). The observation that Coulomb efficiencies of VRFBs approach 100% for high current density even highlights that the same is true for other vanadium species with different oxidation states. Apparently, there is no significant electric-field-driven transport of ionic vanadium species; that is, most of the vanadium crossover is occurring through diffusion of neutral-vanadium-containing species (e.g., $VOSO_4$) entering the membrane as part of excess electrolyte (see also **Figure 2*b***).

The current-independent diffusional flux J_D of vanadium species is then obtained from the current dependence of the Coulomb efficiency (**Figure 6*a***):

$$CE(J) = J/(J + J_D). \qquad 5.$$

For membranes {$sPSO_2$ [sulfonated poly(phenylene sulfone)]} of various thicknesses, J_D linearly decreases with increasing membrane thickness d as expected for a pure diffusional flux (68) (see the inset of **Figure 6*a***). There are reports on the influence of electric field on crossover (e.g., 73) but the supporting data are not robust.

VRFBs therefore constitute a special case of a flow battery whose energy efficiency is controlled by the crossover of neutral vanadium species at low current density and by ohmic losses at high current density. Hence, the two intrinsic properties of materials describing the membrane behavior in this application are the specific diffusional flux $j_D = J_D d$ and the specific conductivity σ. While j_D determines the Coulomb efficiency CE, σ determines the voltage efficiency VE, and the overall energy efficiency is calculated as $EE = CE \cdot VE$. In the following paragraphs, we therefore first discuss separately the parameters controlling j_D and σ.

A common ex situ method for measuring vanadium crossover is to analytically determine vanadium arriving at a, for example, 1 M $MgSO_4$/2 M H_2SO_4 electrolyte separated from a vanadium containing feed electrolyte (e.g., 1 M $VOSO_4$/2 M H_2SO_4) through the membrane in the absence of any osmotic pressure difference across the membrane (74). This method yields the ambipolar diffusion coefficient for, for example, VO^{2+}/Mg^{2+} interdiffusion only, and the membrane's water content cannot be controlled during the experiment. Unfortunately, NMR techniques cannot assess vanadium diffusion coefficients (such as phosphonium diffusion in Nafion; see Section 3.3), but conductivity data bear information about diffusion, because tracer diffusion and ionic mobility are controlled by the same elementary processes. Conductivity is easily measured at a controlled hydration level, and membranes can be converted to the pure VO^{2+} form (standing for all vanadium-containing species). Although VO^{2+} strongly associates with SO_4^{2-} in aqueous solution, it does not associate with sulfonic acid groups of CEMs. Hence, the total conductivity of CEMs in their VO^{2+} form provides direct information about the equivalent conductivity Λ of dissociated vanadyl species. **Figure 6*b*** shows $\Lambda_{VO^{2+}}$ as well as the equivalent conductivity of protons Λ_{H^+} for the two types of membranes (in their pure VO^{2+} and proton forms as a function of water volume fraction Φ_{aq}). The values obtained from extrapolation at $\Phi_{aq} = 1$ coincide with the equivalent conductivity of both species in aqueous solution (75). The data also clearly show that the mobility of both ions is significantly reduced in the less-phase-separated ionomer ($sPSO_2$-360, $IEC = 2.7$ meq g^{-1}) than in the ionomer with well-developed hydrophobic/hydrophilic separation (Nafion, $IEC = 0.94$ meq g^{-1}). When plotting the data against λ, the data plots are almost equal at high water contents, but they decrease faster not only for the less-phase-separated ionomer once the water content falls below a certain limit (see the **Supplemental Material**) but also for the larger species (VO_{aq}^{2+}) at higher water contents compared with the smaller hydrated proton. In other words, the ratio $\Lambda_{H^+}/\Lambda_{VO^{2+}}$ (selectivity) starts increasing below this hydration level (**Figure 6*d***), and this behavior can be exploited to suppress transport of vanadium species while keeping proton conductivity relatively high. For a given degree of phase separation, the controlling parameter is the level of hydration; that is, for less-phase-separated ionomers higher selectivity is achieved even at higher water content. Because the hydration level for a given polymer structure strongly depends on IEC, IEC variations are a means to optimizing selectivity (76, 77). The onset of the increase in selectivity occurs at a width of the aqueous domain nearly equal to the hydrodynamic radius of VO_{aq}^{2+}. This value, ~0.7 nm (**Figure 6*c***), was consistently obtained from its equivalent conductivity (75) and from density functional theory calculations, and it is similar for all other vanadium species present in VRFB electrolytes (78–80).

Supplemental Material >

Because increase in selectivity with respect to mobility is accompanied by a mobility decrease in all species, selectivity and conductivity are clearly related. However, there are parameters affecting only ionic conductivity, and they can be used for optimizing conductivity and with it the energy efficiency of VRFBs.

A widespread approach is to use AEMs to separate electrolytes that contain cations merely as redox-active species (81, 82). The problem with this approach is that in highly concentrated acidic electrolytes, even AEMs become predominant proton conductors, taking up significant amounts of excess electrolyte and therefore also cations and neutral species (15). Because the combined conductivity of anions (SO_4^{2-} in the case of VRFBs) and protons is lower than that of CEMs in the same environment, CEMs are preferred for optimizing ionic conductivity. Then, the focus should be on optimizing the conductivity of protons (present as counterions and part of the excess sulfuric acid) because their mobility is higher than that of anions. The most efficient way to increase proton conductivity of CEMs is to increase their *IEC*. As long as the system is fully dissociated, this proportionally increases the number of protonic charge carriers and the uptake of water, improving percolation within the aqueous ionic domain (note that $\lambda = [H_2O]/[-SO_3H]$ is close to being a constant for a given water activity for *IEC* values that are not too high). This approach is fundamentally limited by the appearance of Manning's counterion condensation (83) when fixed ionic groups are packed too closely, but in most practical cases, the onset of exaggerated swelling or even membrane dissolution defines the maximum feasible *IEC*. Nevertheless, relatively high *IEC* values are acceptable because of the low water activity of VRFB electrolytes. The water uptake of Nafion in this environment is only $\lambda \sim 8$ (compared with $\lambda \sim 20$ in pure water), and even for a high-*IEC* (2.7 meq g^{-1}) poly(phenylene sulfone), water uptake is still acceptably low ($\lambda \sim 9$). Another advantageous aspect of maximizing *IEC* is that it reduces the degree of phase separation (84, 85), keeping the width of the aqueous ionic domains small (see above) provided the hydration number λ is prevented from increasing.

Having discussed phenomena close to thermodynamic equilibrium, we briefly mention irreversible hydrodynamic transport, which is not relevant to a single VRFB cycle but may lead to accumulating effects after repeated cycling. Especially in the case of predominant proton conductivity, strong interaction of protons with the solvent (water) leads to coupled transport of protons and water. In the case of an electric-field-driven proton (hydronium) flux, this leads to electroosmotic water drag, in which the hydrodynamic component increases as the width of the aqueous ionic domain increases (33, 68). If the water drag is not perfectly balanced between charging and discharging, the concentration of one electrolyte increases at the expense of the concentration of the other. Also, other neutral species (e.g., $VOSO_4$) may be dragged by protons, and if the hydrodynamic (collective) component of this transport is high, this could be the reason for a minor indirect electric-field-driven vanadium crossover (73). A recent strategy for mitigating these unwanted effects of electroosmotic drag is to use membranes containing both anions and cations as fixed ionic groups, in which the charge-compensating counterions drag water in opposite directions (86–88). Another option is to keep the width of aqueous ionic domains well below ~1 nm, which not only reduces electroosmotic water drag to less than one H_2O molecule per proton (33) but also minimizes vanadium crossover (see above).

The above considerations suggest the ideal VRFB membrane is an acidic CEM with high *IEC*, albeit with low water uptake, keeping the width of its aqueous ionic domains below ~0.7 nm (i.e., the approximate extension of the relevant hydrated vanadium species). But when it comes to selecting, optimizing, or even developing a membrane for VRFB applications, the details of the device and operating conditions also need to be considered. For example, non-zero-gap setups have significant ohmic resistance contributions stemming from anolyte and catholyte, and setups without forced electrolyte convection show concentration polarization effects at high current density. In the presence of such losses, optimization of membrane conductivity beyond a certain limit is useless. High-current-density operation is possible only with zero-gap, forced-convection setups (89, 90) and highly conducting membranes; for low-current-density applications the focus must be on low vanadium crossover.

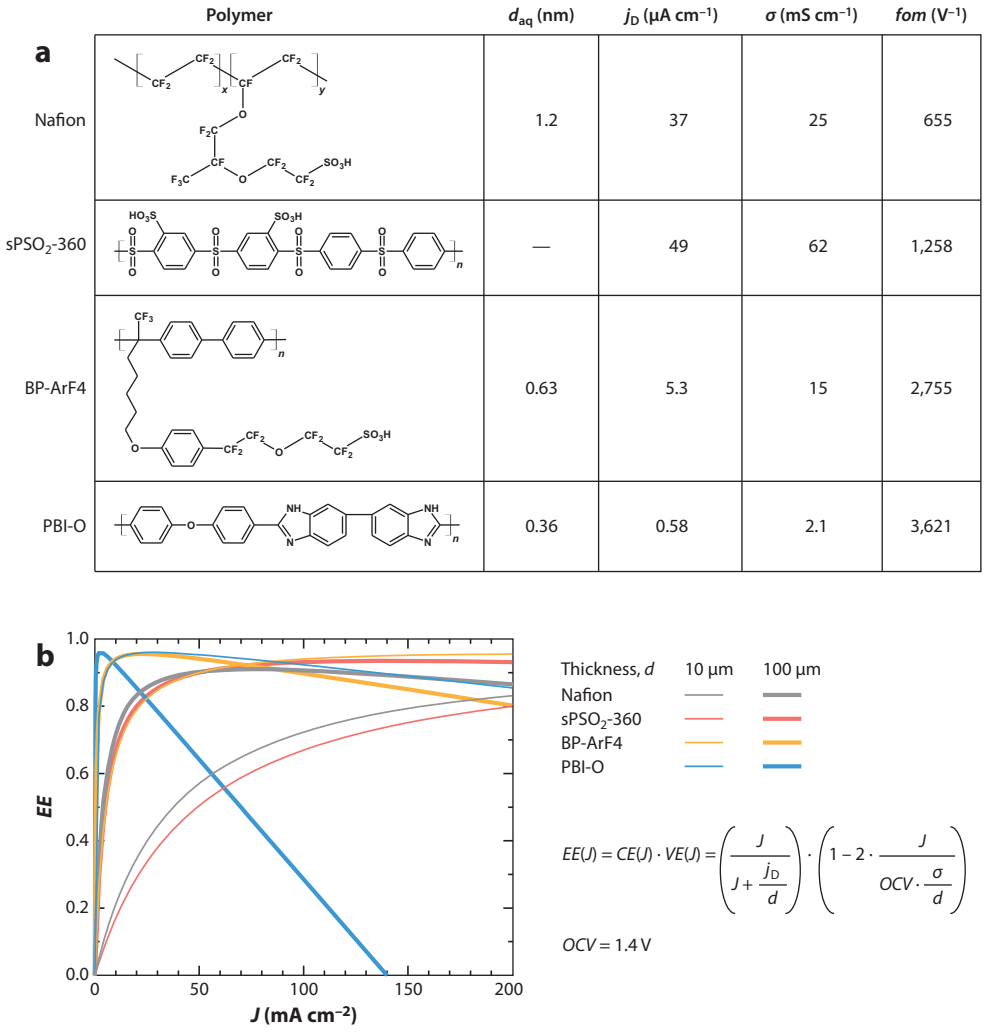

Figure 7

Molecular structure, *IEC*, and width of the aqueous domain d_{aq} under VRFB conditions. (*a*) Specific vanadium crossover current density j_D and membrane-specific conductivity σ are calculated from VRFB test data (68). The $fom = \sigma/j_D$ is also given. (*b*) Because VRFB data were experimentally obtained using membranes of different thicknesses, energy efficiency values calculated for two membrane thicknesses d (10 and 100 μm) are also shown (only losses originating from the membranes are included). Abbreviations: *fom*, figure of merit; *IEC*, ion exchange capacity; PBI, polybenzimidazole; sPSO$_2$, sulfonated poly(phenylene sulfone); VRFB, vanadium-redox-flow battery.

Finally, we briefly discuss four different membrane materials, each representing a certain class of ionomers. For these membrane materials, vanadium crossover current density j_D and membrane-specific conductivity σ were determined in operando with the nonmembrane contributions of the ohmic resistance subtracted (68) (**Figure 7*a***). For a comprehensive compilation of membranes characterized under various conditions, we refer the reader to the supplementary information in Reference 91.

Surprisingly, the membrane PBI-O has the highest figure of merit (*fom*), σ/j_D, of 3,621 (i.e., the best balance of conductivity and crossover). PBI-O is not a true ionomer; it is a neutral polymer, albeit with a high density of basic sites (*IEC* $\sim$ 5 meq g^{-1}). In the presence of highly acidic VRFB electrolytes, basic nitrogen sites get protonated; hence, the polymer is positively charged, keeping anions (HSO_4^- and SO_4^{2-}) adsorbed. The conductivity in this environment then stems mainly from a significant amount (43%) of absorbed excess sulfuric acid, with contributions from protons (H_3O^+) and sulfate anions. One reason why this conductivity ($\sim$1 mS cm^{-1}) remains well below the conductivity of typical ionomer membranes is that the electrolyte is highly dispersed within the polymer, corresponding to narrow electrolyte domains. The clear advantage of this morphology is low specific vanadium crossover ($j_D = 0.58$ μA cm^{-1}) and presumably low electroosmotic water drag (not yet measured). The spongelike microstructure of PBI produced by vapor-induced phase inversion (92) and the introduction of hydrophilic side chains (93) led to an increase of electrolyte uptake and to higher conductivity without much loss of selectivity.

Complementary behavior is observed for a true ionomer with high *IEC*, $sPSO_2$-360. The high concentration of counterions, which are mainly protons in a VRFB environment, and high swelling give this membrane the highest conductivity, which is the primary reason for its high *fom*. Compared with that of PBI-O, the aqueous phase of $sPSO_2$-360 is less dispersed, but the hydrophilic/hydrophobic separation of $sPSO_2$-360 is less developed than that of Nafion (84), which explains why this high-*IEC* hydrocarbon membrane has a higher *fom* (1,258) than Nafion (655) does. Because of its hydrophobic backbone and soft side chain architecture, Nafion has the best-developed phase separation, and even at low electrolyte content (21%) its aqueous domains are wide enough (1.2 nm) to allow for significant vanadium crossover current density $j_D = 34$ μA cm^{-1}. The first rationally designed ionomer membrane is BP-ArF4 (91). Its relatively rigid hydrocarbon backbone and flexible perfluorinated side chains led to the development of narrow and well-defined aqueous domains with an average width just below the extension of hydrated vanadium species ($\sim$0.7 nm). The *fom* of BP-ArF4 (2,755) is higher than that of $sPSO_2$-360, but both transport coefficients σ and j_D are approximately 10 times lower than they are for $sPSO_2$-360. Therefore, VRFB performance of a BP-ArF4 membrane is similar to the performance of a 10-times-thicker $sPSO_2$-360 membrane in the covered range of current densities (see the calculated energy efficiencies in **Figure 7*b***), and the higher *fom* of BP-ArF4 is reflected in a progressively superior performance for the thin BP-ArF4 membrane for higher current density ($I > 200$ mA cm^{-2}). However, j_D and σ do not decrease in the same way when the thickness of the aqueous domain is reduced. This is clearly evidenced by the high *fom* of PBI-O and the trends for absolute conductivity and selectivity as a function of hydration (see **Figures 5** and **6**). One may therefore decide for a thin membrane with highly dispersed electrolytes, but surely there are practical limits to this approach. The highest energy efficiency is expected for a thin 10-μm PBI-O membrane, indeed (**Figure 7*b***), but only for low current density. For current densities higher than $\sim$100 mA cm^{-1}, the higher conductivity of BP-ArF4 makes this ionomer the preferred membrane material.

As explained above, the choice of a suitable membrane material depends on operating conditions (especially current density) and on the ways in which thin membranes can be fabricated [thin membranes supported on porous structures are common (5, 61, 64, 65)]. However, there is also room for optimizing membrane materials: An obvious flaw of PBI-O is that no protons are present as counterions contributing to conductivity, and for $sPSO_2$-360 the swelling is too high to efficiently prevent vanadium crossover. Mitigating strategies are obvious, and there is reasonable hope that we will soon see membranes with enhanced functionality.

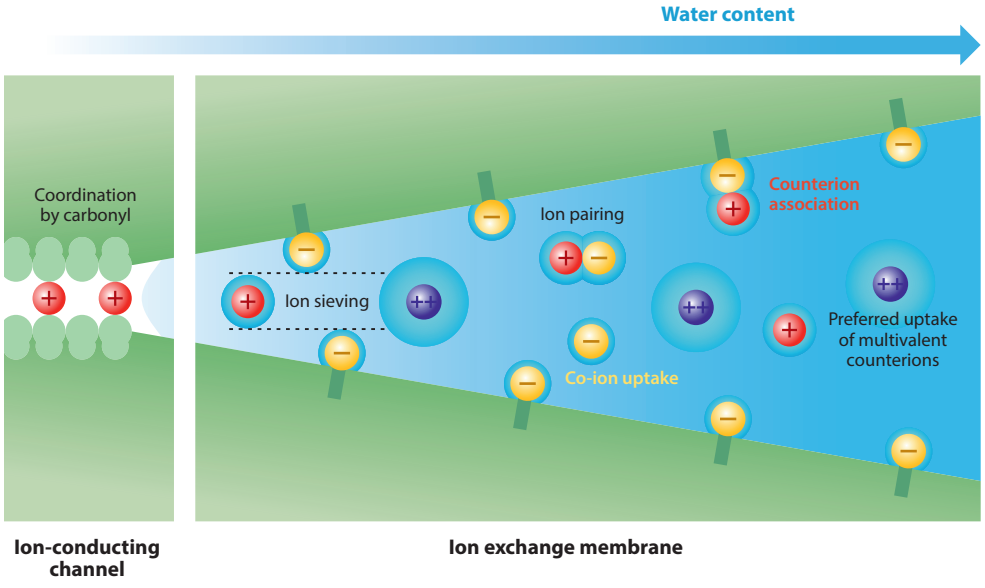

Figure 8

The effects controlling partitioning and mobility of ionic species in ion-conducting channels (dry) and ion (cation) exchange membranes at low and high levels of hydration. In ion-conducting channels, changes in ion coordination are involved, whereas in ion exchange membranes ions remain coordinated by water molecules.

4. SUMMARY

Selective and fast transport of ionic species (ions and their associates) through membranes in contact with aqueous media depends on ion partitioning and ion mobility.

An immediate consequence of the presence of fixed ionic groups, which are part of the structure of IEMs, is electroselectivity [i.e., cation/anion selectivity (CEMs conduct cations and AEMs conduct anions)] and preferential transport of higher-valence ions. Both types of selectivity are consequences of ion partitioning occurring especially at low ionic strength of the aqueous environment and in the absence of ion association. Cation/anion selectivity is a consequence of Donnan exclusion [i.e., co-ion (salt) rejection], and the preferential uptake of higher-valence ions has statistical reasons (minimization of ion concentration gradients).

Another effect is association of a specific type of counterion with fixed ionic groups (**Figure 8**). This not only reduces Donnan exclusion (because of fixed-charge neutralization) but also leads to preferential uptake of this type of counterion over other types. Then, ion immobilization reduces total conductivity but leaves ionic transference numbers virtually unchanged.

Especially under conditions of high ionic strength, low water activity, or both, the most important selectivity mechanism for transport through IEMs is ion sieving (**Figure 8**). With decreasing hydration level (i.e., decreasing width of the aqueous ionic domains), the diffusion of ionic species is progressively restricted through steric effects. These effects depend on the size of the hydrated species—the transport of large species may even come to a standstill, whereas smaller species are still reasonably mobile.

Whereas all transport processes in IEMs take place within aqueous ionic domains, biological systems with selective ion transport are virtually dry (**Figure 8**). For ionophores and ion-conducting protein channels, the stabilizing effect through ion coordination with ligands such as carbonyl or carboxyl groups then compensates for the loss of hydration enthalpy. The stabilizing

effect of both types of coordination shows different dependencies on ionic radius, which is related to electric field strength, electronic polarizability, and electronegativity. This leads to selective uptake of a specific type of ion (circumventing cation ordering, i.e., the mixed alkali effect) and reduces barriers for ion transfer between chemically different coordination cages.

With respect to technical applications, VRFBs constitute a special case in that vanadium crossover is driven mostly by diffusion rather than by ionic current. High-*IEC* acidic CEMs with hydrophobic/hydrophilic phase separation on a small scale and low swelling to keep the width of the aqueous domains below ~0.7 nm (the extension of most hydrated vanadium species) demonstrate the best compromise between low vanadium (and water) crossover and high proton conductivity. For high-current-density applications, the focus should be on high conductivity; at low current density, the good barrier properties of poorly phase-separated membranes made of neutral polymers such as PBI lead to surprisingly good performance. The reason for the latter is because acidic electrolytes are well dispersed in basic PBI-type membranes.

DISCLOSURE STATEMENT

The authors are not aware of any affiliations, memberships, funding, or financial holdings that might be perceived as affecting the objectivity of this review.

ACKNOWLEDGMENTS

We gratefully thank Davide Moia and Rob Usiskin for reading drafts of the article and Jean-Cyrill Kreuer for discussing ion transport in biological systems. We kindly acknowledge financial support by the Bundesministerium für Forschung und Technologie (BMBF) under contract number 03EK3045A.

LITERATURE CITED

1. Dunn B, Farrington GC. 1983. Trivalent ion exchange in beta″ alumina. *Solid State Ionics* 9–10:223–25
2. Foster LM, Anderson MP, Chandrashekhar GV, Burns G, Bradford RB. 1981. The mixed alkali effect in (K, Na)-β-gallate fast ion conductor. *J. Chem. Phys.* 75:2412–22
3. Isard JO. 1969. The mixed alkali effect in glass. *J. Non-Crystalline Solids* 1:235–61
4. Frant MS, Ross JW. 1966. Electrode for sensing fluoride ion activity in solution. *Science* 154:1553–55
5. Luo T, Abdu S, Wessling M. 2018. Selectivity of ion exchange membranes: a review. *J. Membr. Sci.* 555:429–54
6. Sata T, Sata T, Yang W. 2002. Studies on cation-exchange membranes having permselectivity between cations in electrodialysis. *J. Membr. Sci.* 206:31–60
7. Moore C, Pressman BC. 1964. Mechanism of action of valinomycin on mitochondria. *Biochem. Biophys. Res. Commun.* 15:562–67
8. Pioda LAR, Wipf HK, Simon W. 1968. A crystalline complex of potassium rhodanide and valinomycin, an antibiotic of high potassium ion selectivity. EMF measurements on synthetic membranes. *Chimia* 22:189–91
9. Wipf H-K, Olivier A, Simon W. 1970. Mechanismus und Selektivität des Alkali-Ionentransportes in Modell-Membranen in Gegenwart des Antibioticums Valinomycin. 53:1605–8
10. Anderson EL, Bühlmann P. 2016. Electrochemical impedance spectroscopy of ion-selective membranes: artifacts in two-, three-, and four-electrode measurements. *Anal. Chem.* 88:9738–45
11. Bakker E, Bühlmann P, Pretsch E. 1997. Carrier-based ion-selective electrodes and bulk optodes. 1. General characteristics. *Chem. Rev.* 97:3083–132
12. Bühlmann P, Pretsch E, Bakker E. 1998. Carrier-based ion-selective electrodes and bulk optodes. 2. Ionophores for potentiometric and optical sensors. *Chem. Rev.* 98:1593–688
13. Varma S, Sabo D, Rempe SB. 2008. K^+/Na^+ selectivity in K channels and valinomycin: over-coordination versus cavity-size constraints. *J. Mol. Biol.* 376:13–22

14. Varma S, Rogers DM, Pratt LR, Rempe SB. 2011. Design principles for K^+ selectivity in membrane transport. *J. Gen. Physiol.* 137:479–88
15. Münchinger A, Kreuer K-D. 2019. Selective ion transport through hydrated cation and anion exchange membranes I. The effect of specific interactions. *J. Membr. Sci.* 592:117372
16. Elton DC. 2016. *Understanding the dielectric properties of water*. PhD Thesis, Stony Brook Univ., NY
17. Noskov SY, Bernèche S, Roux B. 2004. Control of ion selectivity in potassium channels by electrostatic and dynamic properties of carbonyl ligands. *Nature* 431:830–34
18. Ammann D, Morf WE, Anker P, Meier PC, Pretsch E, Simon W. 1983. Neutral carrier based ion-selective electrodes. In *Ion-Selective Electrode Reviews*, ed. JDR Thomas, pp. 3–92. Oxford, UK: Pergamon
19. Hille B. 2001. *Ionic Channels of Excitable Membranes*. Sunderland, MA: Sinauer
20. Doyle DA, Cabral JM, Pfuetzner RA, Kuo A, Gulbis JM, et al. 1998. The structure of the potassium channel: molecular basis of K^+ conduction and selectivity. *Science* 280:69–77
21. Eisenman G, Latorre R, Miller C. 1986. Multi-ion conduction and selectivity in the high-conductance Ca^{++}-activated K^+ channel from skeletal muscle. *Biophys. J.* 50:1025–34
22. Heginbotham L, MacKinnon R. 1993. Conduction properties of the cloned Shaker K^+ channel. *Biophys. J.* 65:2089–96
23. LeMasurier M, Heginbotham L, Miller C. 2001. KcsA: It's a potassium channel. *J. Gen. Physiol.* 118:303–14
24. Lam YL, Zeng W, Sauer DB, Jiang Y. 2014. The conserved potassium channel filter can have distinct ion binding profiles: structural analysis of rubidium, cesium, and barium binding in NaK2K. *J. Gen. Physiol.* 144:181–92
25. Krasne S. 1978. Ion selectivity in membrane permeation. In *Physiology of Membrane Disorders*, ed. TE Andreoli, JF Hoffman, DD Fanestil, pp. 217–41. Boston: Springer
26. Eisenman G, Horn R. 1983. Ionic selectivity revisited—the role of kinetic and equilibrium process in ion permeation through channels. *J. Membr. Biol.* 76:197–225
27. Dudev T, Lim C. 2014. Ion selectivity strategies of sodium channel selectivity filters. *Acc. Chem. Res.* 47:3580–87
28. Mikhelson K. 2006. AC-impedance studies of ion transfer across ionophore-based ion-selective membranes. *Chem. Anal.* 51:853–67
29. Donnan FG. 1911. Theorie der Membrangleichgewichte und Membranpotentiale bei Vorhandensein von nicht dialysierenden Elektrolyten. Ein Beitrag zur physikalisch-chemischen Physiologie. *Z. Elektrochem. Angew. Phys. Chem.* 17:572–81
30. Teorell T. 1935. An attempt to formulate a quantitative theory of membrane permeability. *Proc. Soc. Exp. Biol. Med.* 33:282–85
31. Meyer KH, Sievers JF. 1936. La perméabilité des membranes I. Théorie de la perméabilité ionique. *Helv. Chim. Acta* 19:649–64
32. Helfferich F. 1959. *Ionenaustauscher: Bd 1: Grundlagen: Struktur, Herstellung, Theorie*. Weinheim, Ger.: Verlag Chemie GmbH
33. Kreuer K-D, Paddison SJ, Spohr E, Schuster M. 2004. Transport in proton conductors for fuel-cell applications: simulations, elementary reactions, and phenomenology. *Chem. Rev.* 104:4637–78
34. Kortüm G. 1966. *Lehrbuch der Elektrochemie*. Weinheim, Ger.: Verlag Chemie GmbH
35. Manning GS. 1979. Counterion binding in polyelectrolyte theory. *Acc. Chem. Res.* 12:443–49
36. Kreuer K-D. 2013. The role of internal pressure for the hydration and transport properties of ionomers and polyelectrolytes. *Solid State Ionics* 252:93–101
37. Zabolotsky VI, Manzanares JA, Nikonenko VV, Lebedev KA, Lovtsov EG. 2002. Space charge effect on competitive ion transport through ion-exchange membranes. *Desalination* 147:387–92
38. Besha AT, Tsehaye MT, Aili D, Zhang WJ, Tufa RA. 2020. Design of monovalent ion selective membranes for reducing the impacts of multivalent ions in reverse electrodialysis. *Membranes* 10:7
39. Oldenburg FJ, Nilsson E, Schmidt TJ, Gubler L. 2019. Tackling capacity fading in vanadium redox flow batteries with amphoteric polybenzimidazole/Nafion bilayer membranes. *ChemSusChem* 12:2620–27
40. Pang X, Tao Y, Xu Y, Pan J, Shen J, Gao C. 2020. Enhanced monovalent selectivity of cation exchange membranes via adjustable charge density on functional layers. *J. Membr. Sci.* 595:117544

41. Abdu S, Martí-Calatayud M-C, Wong JE, García-Gabaldón M, Wessling M. 2014. Layer-by-layer modification of cation exchange membranes controls ion selectivity and water splitting. *ACS Appl. Mater. Interfaces* 6:1843–54
42. Wang YF, Wang SJ, Xiao M, Han DM, Hickner MA, Meng YZ. 2013. Layer-by-layer self-assembly of PDDA/PSS-SPFEK composite membrane with low vanadium permeability for vanadium redox flow battery. *RSC Adv.* 3:15467–74
43. Cheng W, Liu C, Tong T, Epsztein R, Sun M, et al. 2018. Selective removal of divalent cations by polyelectrolyte multilayer nanofiltration membrane: role of polyelectrolyte charge, ion size, and ionic strength. *J. Membr. Sci.* 559:98–106
44. Güler E, van Baak W, Saakes M, Nijmeijer K. 2014. Monovalent-ion-selective membranes for reverse electrodialysis. *J. Membr. Sci.* 455:254–70
45. Marino MG, Melchior JP, Wohlfarth A, Kreuer K-D. 2014. Hydroxide, halide and water transport in a model anion exchange membrane. *J. Membr. Sci.* 464:61–71
46. Yeager HL. 1982. Cation exchange selectivity of a perfluorosulfonate polymer. In *Perfluorinated Ionomer Membranes*, pp. 25–39. Washington, DC: American Chemical Society
47. Bontha JR, Pintauro PN. 1994. Water orientation and ion solvation effects during multicomponent salt partitioning in a Nafion cation-exchange membrane. *Chem. Eng. Sci.* 49:3835–51
48. Yang Y, Pintauro PN. 2000. Multicomponent space-charge transport model for ion-exchange membranes. *AIChE J.* 46:1177–90
49. Pintauro PN, Tandon R, Chao L, Xu W, Evilia R. 1995. Equilibrium partitioning of monovalent divalent cation-salt mixtures in Nafion cation-exchange membranes. *J. Phys. Chem.* 99:12915–24
50. Okada T, Arimura N, Satou H, Yuasa M, Kikuchi T. 2005. Membrane transport characteristics of binary cation systems with Li^+ and alkali metal cations in perfluorosulfonated ionomer. *Electrochim. Acta* 50:3569–75
51. Tessman JR, Kahn AH, Shockley W. 1953. Electronic polarizabilities of ions in crystals. *Phys. Rev.* 92:890–95
52. Volkov VI, Pavlov AA, Sanginov EA. 2011. Ionic transport mechanism in cation-exchange membranes studied by NMR technique. *Solid State Ionics* 188:124–28
53. Geise GM, Cassady HJ, Paul DR, Logan BE, Hickner MA. 2014. Specific ion effects on membrane potential and the permselectivity of ion exchange membranes. *Phys. Chem. Chem. Phys.* 16:21673–81
54. Nibel O, Rojek T, Schmidt TJ, Gubler L. 2017. Amphoteric ion-exchange membranes with significantly improved vanadium barrier properties for all-vanadium redox flow batteries. *ChemSusChem* 10:2767–77
55. Glueckauf E. 1955. The influence of ionic hydration on activity coefficients in concentrated electrolyte solutions. *Trans. Faraday Soc.* 51:1235–44
56. Ruthven DM. 1977. Diffusion in molecular sieves: a review of recent developments. In *Molecular Sieves–II*, ed. JR Katzer, pp. 320–34. Washington, DC: American Chemical Society
57. Kreuer K-D, Weppner W, Rabenau A. 1982. Proton conduction in zeolites. *Mater. Res. Bull.* 17:501–9
58. Xu Z, Michos I, Wang XR, Yang RD, Gu XH, Dong JH. 2014. A zeolite ion exchange membrane for redox flow batteries. *Chem. Commun.* 50:2416–19
59. Dai WJ, Shen Y, Li ZH, Yu LH, Xi JY, Qiu XP. 2014. SPEEK/graphene oxide nanocomposite membranes with superior cyclability for highly efficient vanadium redox flow battery. *J. Mater. Chem. A* 2:12423–32
60. Wu C, Bai H, Lv Y, Lv Z, Xiang Y, Lu S. 2017. Enhanced membrane ion selectivity by incorporating graphene oxide nanosheet for vanadium redox flow battery application. *Electrochim. Acta* 248:454–61
61. Kim S, Choi J, Choi C, Heo J, Kim DW, et al. 2018. Pore-size-tuned graphene oxide frameworks as ion-selective and protective layers on hydrocarbon membranes for vanadium redox-flow batteries. *Nano Lett.* 18:3962–68
62. Ren CE, Hatzell KB, Alhabeb M, Ling Z, Mahmoud KA, Gogotsi Y. 2015. Charge- and size-selective ion sieving through $Ti_3C_2T_x$ MXene membranes. *J. Phys. Chem. Lett.* 6:4026–31
63. Zhang H, Zhang H, Li X, Mai Z, Zhang J. 2011. Nanofiltration (NF) membranes: the next generation separators for all vanadium redox flow batteries (VRBs)? *Energy Environ. Sci.* 4:1676–79
64. Wang P, Wang M, Liu F, Ding S, Wang X, et al. 2018. Ultrafast ion sieving using nanoporous polymeric membranes. *Nat. Commun.* 9:569

65. Dai Q, Liu Z, Huang L, Wang C, Zhao Y, et al. 2020. Thin-film composite membrane breaking the trade-off between conductivity and selectivity for a flow battery. *Nat. Commun.* 11:13
66. Kim S, Yan J, Schwenzer B, Zhang J, Li L, et al. 2010. Cycling performance and efficiency of sulfonated poly(sulfone) membranes in vanadium redox flow batteries. *Electrochem. Commun.* 12:1650–53
67. Kreuer K-D, Portale G. 2013. A critical revision of the nano-morphology of proton conducting ionomers and polyelectrolytes for fuel cell applications. *Adv. Funct. Mater.* 23:5390–97
68. Münchinger A. 2021. *Selective ion transport through ion exchange membranes—effects of chemical interactions and morphology*. PhD Thesis, Univ. Stuttgart, Ger.
69. Schmidt O, Hawkes A, Gambhir A, Staffell I. 2017. The future cost of electrical energy storage based on experience rates. *Nat. Energy* 2:17110
70. Noack J, Roznyatovskaya N, Herr T, Fischer P. 2015. The chemistry of redox-flow batteries. *Angew. Chem. Int. Ed.* 54:9776–809
71. Mögelin H, Yao G, Zhong H, dos Santos AR, Barascu A, et al. 2018. Porous glass membranes for vanadium redox-flow battery application—effect of pore size on the performance. *J. Power Sourc.* 377:18–25
72. Li X-R, Qin Y, Xu W-G, Liu J-G, Yang J-Z, et al. 2016. Thermodynamic investigation of electrolytes of the vanadium redox flow battery (V): conductivity and ionic dissociation of vanadyl sulfate in aqueous solution in the 278.15–318.15 K temperature range. *J. Solut. Chem.* 45:1879–89
73. Darling RM, Weber AZ, Tucker MC, Perry ML. 2015. The influence of electric field on crossover in redox-flow batteries. *J. Electrochem. Soc.* 163:A5014–22
74. Sun C, Chen J, Zhang H, Han X, Luo Q. 2010. Investigations on transfer of water and vanadium ions across Nafion membrane in an operating vanadium redox flow battery. *J. Power Sourc.* 195:890–97
75. Kohler G, Wendt H. 1966. Die Bestimmung von Gleichgewichtskonstanten aus kinetischen Messungen. *Ber. Bunsen-Ges. Phys. Chem.* 70:674–81
76. Chen D, Chen X, Ding L, Li X. 2018. Advanced acid-base blend ion exchange membranes with high performance for vanadium flow battery application. *J. Membr. Sci.* 553:25–31
77. Zhang Y, Zheng L, Liu B, Wang H, Shi H. 2019. Sulfonated polysulfone proton exchange membrane influenced by a varied sulfonation degree for vanadium redox flow battery. *J. Membr. Sci.* 584:173–80
78. Sepehr F, Paddison SJ. 2013. The solvation structure and thermodynamics of aqueous vanadium cations. *Chem. Phys. Lett.* 585:53–58
79. Hinkle KR, Jameson CJ, Murad S. 2014. Transport of vanadium and oxovanadium ions across zeolite membranes: a molecular dynamics study. *J. Phys. Chem. C* 118:23803–10
80. Liu Z, Li R, Chen J, Wu X, Zhang K, et al. 2017. Theoretical investigation into suitable pore sizes of membranes for vanadium redox flow batteries. *ChemElectroChem* 4:2184–89
81. Chen D, Hickner MA, Agar E, Kumbur EC. 2013. Optimized anion exchange membranes for vanadium redox flow batteries. *ACS Appl. Mater. Interfaces* 5:7559–66
82. Choi H-S, Oh Y-H, Ryu C-H, Hwang G-J. 2014. Characteristics of the all-vanadium redox flow battery using anion exchange membrane. *J. Taiwan Inst. Chem. Eng.* 45:2920–25
83. Manning GS. 1969. Limiting laws and counterion condensation in polyelectrolyte solutions I. Colligative properties. *J. Chem. Phys.* 51:924–33
84. de Araujo CC, Kreuer K-D, Schuster M, Portale G, Mendil-Jakani H, et al. 2009. Poly(p-phenylene sulfone)s with high ion exchange capacity: ionomers with unique microstructural and transport features. *Phys. Chem. Chem. Phys.* 11:3305–12
85. Kreuer K-D. 2014. Ion conducting membranes for fuel cells and other electrochemical devices. *Chem. Mater.* 26:361–80
86. Oldenburg FJ, Schmidt TJ, Gubler L. 2017. Tackling capacity fading in vanadium flow batteries with amphoteric membranes. *J. Power Sourc.* 368:68–72
87. Gubler L. 2019. Membranes and separators for redox flow batteries. *Curr. Opin. Electrochem.* 18:31–36
88. Liu L, Wang C, He Z, Das R, Dong B, et al. 2021. An overview of amphoteric ion exchange membranes for vanadium redox flow batteries. *J. Mater. Sci. Technol.* 69:212–27
89. Aaron DS, Liu Q, Tang Z, Grim GM, Papandrew AB, et al. 2012. Dramatic performance gains in vanadium redox flow batteries through modified cell architecture. *J. Power Sourc.* 206:450–53
90. Ulaganathan M, Aravindan V, Yan Q, Madhavi S, Skyllas-Kazacos M, Lim TM. 2016. Recent advancements in all-vanadium redox flow batteries. *Adv. Mater. Interfaces* 3:1500309

91. Wang T, Han J, Kim K, Münchinger A, Gao Y, et al. 2020. Suppressing vanadium crossover using sulfonated aromatic ion exchange membranes for high performance flow batteries. *Mater. Adv.* 1:2206–18
92. Yuan Z, Duan Y, Zhang H, Li X, Zhang H, Vankelecom I. 2016. Advanced porous membranes with ultrahigh selectivity and stability for vanadium flow batteries. *Energy Environ. Sci.* 9:441–47
93. Peng S, Wu X, Yan X, Gao L, Zhu Y, et al. 2018. Polybenzimidazole membranes with nanophase-separated structure induced by non-ionic hydrophilic side chains for vanadium flow batteries. *J. Mater. Chem. A* 6:3895–905